Surface roughening in low-pressure chemical vapor deposition

Jason T. Drotar, Y.-P. Zhao, T.-M. Lu, and G.-C. Wang
Department of Physics, Applied Physics, and Astronomy, Rensselaer Polytechnic Institute, Troy, New York 12180-3590
(Received 1 May 2001; revised manuscript received 18 June 2001; published 10 September 2001)

We examine, using $(2+1)$-dimensional Monte Carlo simulations, the roughening behavior of a reemission model for chemical vapor deposition. We find that, for pure first-order reemission, the interface roughens logarithmically with time and that the scaling exponents are, for most sets of conditions, close to the exponents of the Edwards-Wilkinson model ($\alpha=0$, $\beta=0$, and $z=2$). We compare our results to experimental results on chemical vapor deposition.

DOI: 10.1103/PhysRevB.64.125411 PACS number(s): 68.55.Jk, 05.40.−a, 05.45.−a, 68.35.Ct

I. INTRODUCTION

Chemical vapor deposition (CVD) is a very important thin-film deposition technique in the microelectronics industry and other industries that make use of thin-film coatings. The CVD process includes precursor transport, chemical reactions, and surface interactions. There are two limiting cases for CVD: the high-pressure and low-pressure CVD processes. For the high-pressure CVD process, the mean free path of the precursor is much smaller than the characteristic length of the surface features. In other words, the Knudsen number (defined as the ratio of the mean free path of the precursor to the characteristic length of the surface features) is small. Therefore the high-pressure CVD process is a hydrodynamic process. For low-pressure CVD (LPCVD), since the mean free path of the precursor is much larger than the characteristic length of the surface features, the process can be described by ballistic transport.

Several researchers have studied surface morphology or morphological stability issues for the small Knudsen number case (pressure ~10–760 Torr).[1–6] In these studies, gas transport was taken into account by using a continuum diffusion equation, and it was assumed that the gas-film interface reaches quasithermal equilibrium. In other words, the effects of surface diffusion, gas diffusion, capillarity, surface reactions, and the curvature of the film are all taken into account in the framework of continuum theory. Particularly, Bales *et al.* have shown theoretically that, in the diffusion-limited growth regime, the surface is not stable and has a fingerlike morphology.[3] In the reaction-limited growth regime, the surface should, theoretically, exhibit Kardar-Parisi-Zhang (KPZ) type growth,[7] but so far there has been no experimental evidence to support this claim. This could be due to complications caused by flow transport.

In the large-Knudsen-number case, i.e., the LPCVD process, researchers have used the idea of ballistic transport of an ideal gas to study trench or via filling problems for many years.[7–14] They have shown that, since the Knudsen number is large, collisions of precursors within the trench or via can be neglected. This kind of line-of-sight model can explain very well the features observed in trench evolution, although the details of the model may vary. However, surface morphological evolution governed by this kind of dynamics has only recently been studied.[15]

Recently, we have demonstrated that a reemission model, for large Knudsen number, can explain the unusual scaling behavior observed in plasma etching.[16,17] In this model, we applied the same ideas that had been presented in the line-of-sight model for LPCVD. In other words, during plasma etching, the pressure is usually low enough so that the mean free path of the vapor particles is much larger than the size of the surface features. In this case, collisions between vapor particles can be ignored, and the particles are assumed to travel in a straight line until striking the surface. Clearly, the same type of model can also be applied to describe the LPCVD process.

In this paper, we present the results of Monte Carlo simulations that demonstrate the scaling behavior of the reemission model for the case of deposition (corresponding to LPCVD). We also discuss the relationship of these results to other theoretical models of surface roughening. Finally, we compare our results to experimental results of low-pressure chemical vapor deposition.

II. MODEL

In the reemission model, particles are incident on a surface (which we initially take to be flat) and, upon colliding with the surface, a particle either sticks on the surface or is reemitted and goes elsewhere. This is shown in Fig. 1. When a particle sticks on the surface, it will either etch the surface (for the case of etching) or deposit on it (for the case of deposition). A reemitted particle will simply go off in some direction and may collide with the surface again. We call

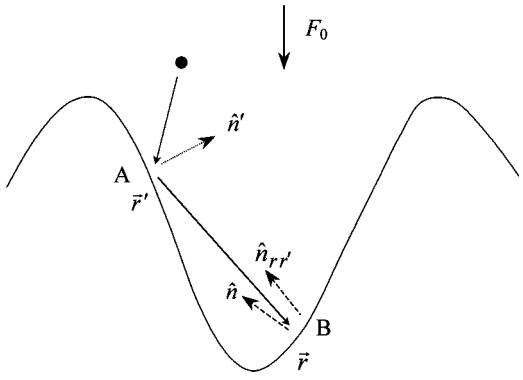

FIG. 1. Flux reemission: the incoming particle can be reemitted from point *A* to land at point *B*.

incident particles zeroth-order particles, while an nth-order particle that has been reemitted is called an $(n+1)$th-order particle. An nth-order particle has a probability s_n of sticking, where s_n is called the nth-order sticking coefficient. A reemission process is characterized by, among other things, its sticking coefficients. In particular, we define an nth-order reemission process by $s_i \approx 0$ for $i<n$ and $s_n=1$.

To model LPCVD, we assume first-order reemission deposition. There are still several unknowns, however. First, one must specify the properties of the incident flux. For example, the flux can be collimated, in which case the incoming particles come from a single direction, or it can be noncollimated, in which case the incoming particles come from a range of directions. We consider only two cases. In the first case, called directional flux, the incoming particles come from the normal direction only. In the second case, called nondirectional flux, incoming particles can come from any direction and obey the probability distribution

$$\frac{dP}{d\Omega}=\frac{\cos\theta}{\pi}, \tag{1}$$

where the angle θ is measured with respect to the substrate normal. This distribution is derived from the assumption that incoming particles come from a gas containing particles traveling in all directions with equal probability.

The next thing one must specify is the mode of reemission. For example, when a particle is reemitted, the direction it goes off in can depend on the direction from which it came. This case is called nondiffuse reemission. One can also have diffuse reemission. This is the case if the direction in which the particle leaves does not depend on the direction from which it came. There are actually many different kinds of diffuse and nondiffuse reemission, but we focus only on three specific cases. The first two, thermal and uniform, are considered diffuse reemission. The last, specular, is a type of nondiffuse reemission. For thermal reemission, the probability distribution (probability per solid angle) of the reemitted flux is given by $P=(\hat{\mathbf{n}}_{\mathbf{r}'\mathbf{r}}\cdot\hat{\mathbf{n}}')/\pi$, while, for uniform reemission, it is given by $P=1/2\pi$. The unit normal vector at the place the flux is being reemitted from is $\hat{\mathbf{n}}'$, while $\hat{\mathbf{n}}_{\mathbf{r}'\mathbf{r}}$ is a unit vector that points in the direction the flux goes off in (see Fig. 1). For specular reemission, the outgoing flux angle is equal to the incident angle.

In previous work, we used the continuum equation

$$\frac{\partial h}{\partial t}=v\nabla^2 h-\kappa\nabla^4 h\mp\sqrt{1+(\nabla h)^2}\times[s_0F_0(\mathbf{r},t)+s_1F_1(\mathbf{r},t)+\cdots]+\eta \tag{2}$$

to describe the reemission model and solved this equation numerically.[16,18] This equation describes the evolution of the surface height $h(x,y)$. The first term corresponds to condensation and evaporation, and the second term is due to surface diffusion. The last term is a noise term, which accounts for the fact that the incoming particles arrive at random times and at random positions. The third term is due to reemission, and the $\sqrt{1+(\nabla h)^2}$ factor is present because growth occurs normal to the local surface. Also present are terms of the form s_nF_n, where F_n is the flux of nth-order particles. Note that F_0 is simply the incident flux. As discussed in Ref. 18, the higher-order fluxes can be found recursively from the lower-order fluxes.

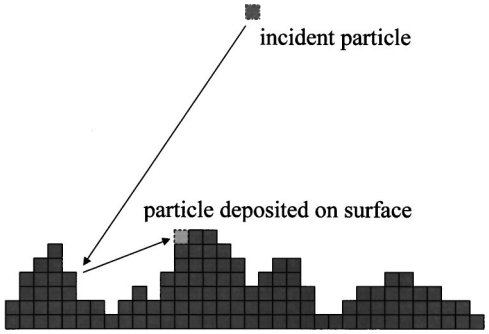

FIG. 2. The Monte Carlo simulation of the reemission model: an incoming particle bounces off the surface and then deposits elsewhere on the surface.

In a previous study, we found that Monte Carlo simulations of the reemission model were much more efficient than numerically solving Eq. (2).[16,18] Therefore, in the present work, we use only Monte Carlo simulations. The idea behind the Monte Carlo simulations is simple. The surface is assumed to be described by a height function $h(x,y)$ defined on a periodic $N\times N$ lattice. Furthermore, h can take on only integer values. The periodic boundary condition of the lattice implies that $h(x+iN,y+jN)=h(x,y)$ for any integers i,j. The simulation proceeds one particle at a time. First, a random position in the x-y plane is chosen for the particle. The initial position of the particle in the h direction is always one position higher than the maximum of the surface. Next, the direction that the particle will go off in is chosen; the distribution of directions depends on the properties of the incident flux. The particle moves in this direction until hitting the surface, after which it can deposit on the surface or be reemitted according to the reemission mode. If it is reemitted, the particle will travel until it hits the surface again or passes above the highest point on the surface. Once the particle has deposited on the surface or has passed above the highest point on the surface (meaning it will never hit the surface), the above procedure is repeated for a new particle. This procedure is illustrated in Fig. 2. Also, to avoid overhangs, a particle that hits the side of a column will slide down the column before sticking.

The above procedure allows us to generate simulated surfaces for the reemission model. Once this is done, it is necessary to describe the evolution of the generated surfaces quantitatively. From the simulated surfaces, one can compute the time dependent height-height correlation function

$$H(\mathbf{r},t)=\langle[h(\mathbf{r}+\mathbf{r}',t)-h(\mathbf{r}',t)]^2\rangle, \tag{3}$$

which contains most of the relevant statistical information about the surfaces. The averaging is done over the $\mathbf{r}'$ variable. We assume that the height-height correlation function has the form[19]

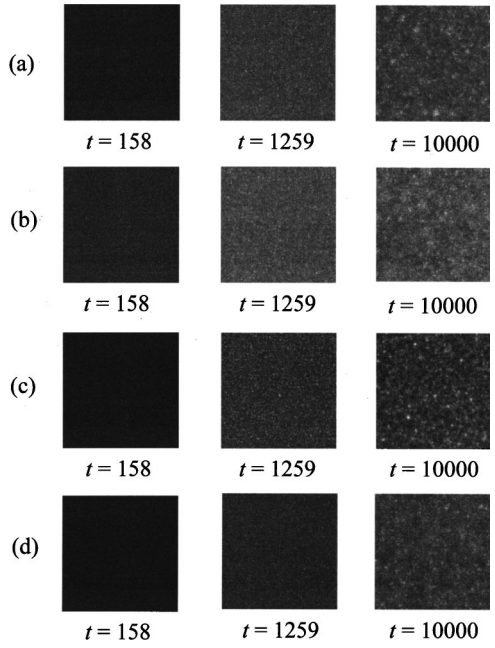

FIG. 3. Simulated surfaces for first-order deposition at various times. (a) Nondirectional flux and thermal reemission, (b) nondirectional flux and uniform reemission, (c) nondirectional flux and specular reemission, and (d) directional flux and thermal reemission. The gray scale is adjusted so that the highest point on the surface is white and the lowest point is black.

$$H(\mathbf{r},t)=2[w(t)]^2 f\left[\frac{r}{\xi(t)}\right], \tag{4}$$

with $f(r)\propto r^{2\alpha}$ for $r\ll 1$ and $f(r)=1$ for $r\gg 1$. Here $w(t)$ is the interface width defined by $w(t)^2=\langle[h(\mathbf{r},t)-\overline{h}(t)]^2\rangle$, where $\overline{h}(t)$ is the average height of the surface and the average is over all $\mathbf{r}$, $\xi(t)$ is the lateral correlation length, and α is called the roughness exponent. We assume that these parameters can characterize a single surface completely. By looking at how these parameters evolve with time, one can also characterize the dynamic behavior of a model. We assume that both $w(t)$ and $\xi(t)$ evolve in time as power laws,

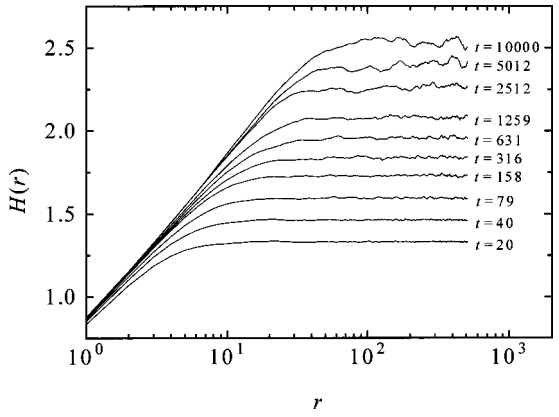

FIG. 4. Height-height correlation functions for various times for the 1024×1024 Monte Carlo simulation of first-order deposition with nondirectional flux and thermal reemission.

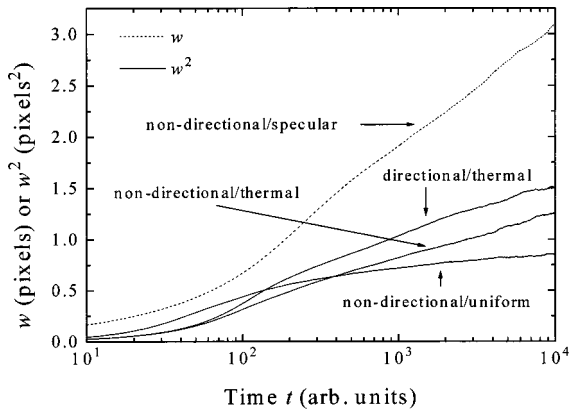

FIG. 5. Interface width squared vs time for the 1024×1024 Monte Carlo simulations of first-order deposition for different types of reemission and incident flux. For the case of nondirectional flux and specular reemission, the interface width vs time has been plotted.

$$w\propto t^{\beta} \tag{5}$$

and

$$\xi\propto t^{1/z}, \tag{6}$$

where β and z are the growth and dynamic exponents, respectively. The parameters α, β, and z are not independent, but are assumed to satisfy

$$z=\alpha/\beta. \tag{7}$$

III. RESULTS AND DISCUSSION

For the case of pure first-order deposition, simulations were carried out with a 1024×1024 lattice. The sticking coefficients used were $s_0=0.05$ and $s_1=1$, and four different cases were simulated: nondirectional flux and thermal reemission, nondirectional flux and uniform reemission, nondirectional flux and specular reemission, and directional flux and thermal reemission. Simulated surfaces at different times, for each case, are shown in Fig. 3. The time is scaled

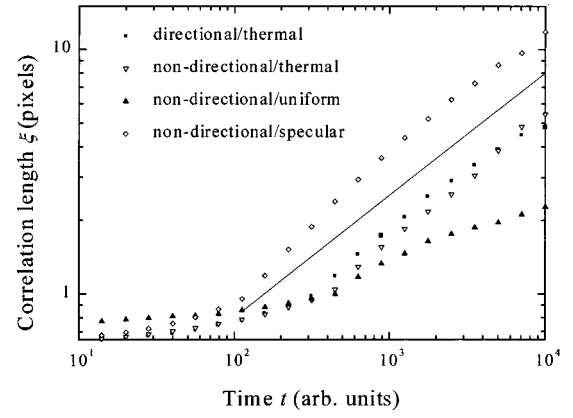

FIG. 6. Correlation length vs time for the 1024×1024 Monte Carlo simulations of first-order deposition for different types of reemission and incident flux. The solid line corresponds to $\xi\propto t^{1/2}$.

TABLE I. The predicted scaling exponents for several different $(2+1)$-dimensional growth and etching models. For comparison, experimental results for low-pressure chemical vapor deposition (LPCVD) and plasma-enhanced chemical vapor deposition (PECVD) are also shown.

Model		α	β	z	Reference
Random deposition		Not defined	0.5	Not defined	20
Edwards-Wilkinson		0	0	2	20
KPZ		0.38	0.24	1.58	21
Mullins diffusion		1	0.25	4	22
Shadowing growth		Not defined	1	1.08 ± 0.1	23
Shadowing etching		0	0	0	23
First-order reemission etching		~1	~1	~1	16,18
First-order reemission deposition	nondir/thermal	~0	~0	1.89	This work
	nondir/uniform	~0	~0	4.76	
	nondir/specular	0.41	~0	2.08	
	dir/thermal	~0	~0	2.33	
LPCVD of *a*-Si on Si		0.48			24
LPCVD of poly-Si on Si		0.90			24
LPCVD of Cu on Si(100) at 453 K		0.81 ± 0.05	0.62 ± 0.09		25
LPCVD of SiO_2 on Si(100)	611 K	0.58	0.51		26
	723 K	0.42	0.26	1.61	
PECVD of *a*-Si:H on Si(100) at 523 K			0.11	7.7	27
PECVD of *a*-Si:H on Si(001)	323 K		0.54 ± 0.03		28
	523 K		0.38 ± 0.03		
	613 K		0.36 ± 0.03		
PECVD of *a*-Si:H on graphite at 573 K			0.20		29
PECVD of *a*-Si:H on Si(100)	373 K		0.42		30
	473 K		0.29		
	523 K		0.29		
	573 K		0.11		
	723 K		0.17		
	773 K		0.07		

so that each simulation ends at 10 000, and the total number of incident particles is 500×10^6. The surface morphology, in each case, is rough, and the correlation length increases with time. The morphology for the case of nondirectional flux and specular reemission [Fig. 3(c)] appears to be slightly different from the other three. In Fig. 4, we plot the height-height correlation function for different times for the case of nondirectional flux and thermal reemission. The plot is in semilogarithmic scale and is almost a straight line, at later times, for $r\ll\xi$. This implies that $H(r)\propto\ln(r)$ for $r\ll\xi$, which means that $\alpha\approx0$. We also find that $\alpha\approx0$ for nondirectional flux and uniform reemission and directional flux and thermal reemission. For nondirectional flux and specular reemission, we find that $\alpha=0.41$.

In Fig. 5, we plot the interface width versus time for the case of nondirectional flux and specular reemission, and we plot the square of the interface width versus time for the remaining three cases. In Fig. 6, we plot the correlation length versus time for all four cases. The first plot is in semilogarithmic scale, while the second plot is in log-log scale, and in both plots, we can see an initial crossover regime followed by a late-time scaling regime. The crossover takes considerable time, and the scaling regime is only observed from about $t=1000$ to $t=10\,000$. From Fig. 5, it appears that that $w\propto\ln(t)$ in the scaling regime, for the case of nondirectional flux and specular reemission. For the remaining cases, it appears that $w^2\propto\ln(t)$ in the scaling regime. However, in each case, we conclude that $\beta\approx0$. In Fig. 6, we see a power-law dependence of the correlation length on time, from which we can obtain the dynamic exponent. The exponents for first-order reemission are summarized in Table I along with the exponents for several other growth and etching models. Some experimental results are also shown. Note that the exponents for the Edwards-Wilkinson model are close to the results we obtained for first-order reemission growth for most sets of conditions. However, the growth mechanism for the Edwards-Wilkinson model is completely different from the mechanism for the reemission model. This illustrates the fact that universality classes and their exponents do not have a one-to-one correspondence.

From the experimental results in Table I, we see that the exponents found for LPCVD, for most cases, do not agree with our results for first-order reemission growth. There are at least two possible explanations for this. First, other mechanisms might be present, aside from reemission. For example, surface diffusion could be responsible for the higher value of α found in some CVD experiments. Second, the reemission in the CVD experiments might not be first order. Recently, we have examined the behavior of the reemission model for cases other than first-order reemission.[15] For example, we examined the case where all sticking coefficients are equal (all-order reemission) and examined the transition from first-order reemission to zeroth-order reemission (shadowing) that occurs when s_0 is increased.[15] We discovered that the scaling exponents undergo a transition that is qualitatively similar to the transition in experimental CVD exponents that occurs when substrate temperature is increased.[15] Thus it is likely that first-order reemission holds for LPCVD only at high temperatures.

IV. CONCLUSION

Our Monte Carlo simulations show that first-order reemission deposition gives scaling exponents similar to the exponents of the Edwards-Wilkinson model, in sharp contrast to first-order reemission etching. While first-order reemission deposition does exhibit some degree of universality, the universality is not as strong as in the case of first-order reemission etching. Also, we find poor agreement between our first-order reemission deposition simulations and chemical vapor deposition experiments, especially for low temperatures. This is probably due to the high value of the sticking coefficient that exists for low temperatures.

ACKNOWLEDGMENT

This work is supported by the NSF.

[1] C. H. J. van den Brekel and A. K. Jansen, J. Cryst. Growth **43**, 364 (1978); **43**, 371 (1978).
[2] B. J. Palmer and R. G. Gordon, Thin Solid Films **158**, 313 (1988); **177**, 141 (1989).
[3] G. S. Bales, A. C. Redfield, and A. Zangwill, Phys. Rev. Lett. **62**, 776 (1989).
[4] R. Ananth and W. N. Gill, J. Cryst. Growth **118**, 60 (1992).
[5] H. J. Viljoen, J. J. Thiart, and V. Hlavacek, AIChE J. **40**, 1032 (1994).
[6] C.-C. Hwang, H.-Y. Yang, J.-Y. Hsieh, and Y.-M. Dai, Thin Solid Films **304**, 371 (1997).
[7] M. Ikegawa and J. Kobayashi, J. Electrochem. Soc. **136**, 2982 (1989).
[8] M. J. Cooke and G. Harris, J. Vac. Sci. Technol. A **7**, 3217 (1989).
[9] T. S. Cale and G. B. Raupp, J. Vac. Sci. Technol. B **8**, 649 (1990); **8**, 1242 (1990).
[10] J. J. Hsieh, J. Vac. Sci. Technol. A **11**, 78 (1993).
[11] V. K. Singh and S. G. Shaqfeh, J. Vac. Sci. Technol. A **11**, 557 (1993).
[12] D. G. Coronell and K. F. Jensen, J. Electrochem. Soc. **141**, 2545 (1994).
[13] S. T. Rodgers and K. F. Jensen, J. Appl. Phys. **83**, 524 (1998).
[14] T. S. Cale and V. Mahadev, in *Modeling of Film Deposition for Microelectronic Applications*, edited by S. Rossnagel and A. Ulman (Academic, San Diego, 1996).
[15] Y.-P. Zhao, Jason T. Drotar, G.-C. Wang, and T.-M. Lu, Phys. Rev. Lett. (to be published).
[16] Y.-P. Zhao, Jason T. Drotar, G.-C. Wang, and T.-M. Lu, Phys. Rev. Lett. **82**, 4882 (1999).
[17] Pascal Brault, Philippe Dumas, and Franck Salvan, J. Phys.: Condens. Matter **10**, L27 (1998).
[18] Jason T. Drotar, Y.-P. Zhao, G.-C. Wang, and T.-M. Lu, Phys. Rev. B **61**, 3012 (2000).
[19] F. Family and T. Vicsek, J. Phys. A **18**, L75 (1985); F. Family, Physica A **168**, 561 (1990).
[20] A.-L. Barabási and H. E. Stanley, *Fractal Concepts in Surface Growth* (Cambridge University Press, Cambridge, England, 1995).
[21] M. Kardar, G. Parisi, and Y.-C. Zhang, Phys. Rev. Lett. **56**, 889 (1986); J. G. Amar and F. Family, Phys. Rev. A **41**, 3399 (1990); K. Moser, D. E. Wolf, and J. Kertész, Physica A **178**, 215 (1991).
[22] F. Family, J. Phys. A **19**, L441 (1986); Jacques G. Amar, Pui-Man Lam, and Fereydoon Family, Phys. Rev. E **47**, 3242 (1993).
[23] R. P. U. Karunasiri, R. Bruinsma, and K. Rudnick, Phys. Rev. Lett. **62**, 788 (1989); Jian Hua Yao and Hong Guo, Phys. Rev. E **47**, 1007 (1993); Christopher Roland and Hong Guo, Phys. Rev. Lett. **66**, 2104 (1991); G. S. Bales and A. Zangwill, *ibid.* **63**, 692 (1989); Jason T. Drotar, Y.-P. Zhao, T.-M. Lu, and G.-C. Wang, Phys. Rev. B **62**, 2118 (2000).
[24] T. Yoshinobu, A. Iwamoto, K. Sudoh, and H. Iwasaki, in *Fractal Aspects of Materials*, edited by Fereydoon Family, Paul Meakin, Bernard Sapoval, and Richard Wool, Mater. Res. Soc. Symp. Proc. No. **367** (Materials Research Society, Pittsburgh, 1995), p. 329.
[25] L. Vázquez, J. M. Albella, R. C. Salvarezza, A. J. Arvia, R. A. Levy, and D. Perese, Appl. Phys. Lett. **68**, 1285 (1996).
[26] Fernando Ojeda, Rodolfo Cuerno, Roberto Salvarezza, and Luis Vázquez, Phys. Rev. Lett. **84**, 3125 (2000).
[27] D. M. Tanenbaum, A. L. Laracuente, and A. Gallagher, Phys. Rev. B **56**, 4243 (1997).
[28] M. Kondo, T. Ohe, K. Saito, T. Nishimiya, and A. Matsuda, J. Non-Cryst. Solids **227–230**, 890 (1998).
[29] K. Ikuta, Y. Toyoshima, S. Yamasaki, A. Matsuda, and K. Tanaka, in *Amorphous Silicon Technology*, edited by Michael Hack, Eric A. Schiff, Sigurd Wagner, Ruud Schropp, and Akihisa Matsuda, Mater. Res. Soc. Symp. Proc. No. **420** (Materials Research Society, Pittsburgh, 1996), p. 413.
[30] A. Smets, E. Kessels, B. Korevaar, C. Smit, R. van de Sanden, and D. Schram (unpublished).